Palladium-Catalyzed *Meta*-Selective C−H Bond Activation with a Nitrile-Containing Template: Computational Study on Mechanism and Origins of Selectivity

Yun-Fang Yang,[†,‡,⊥] Gui-Juan Cheng,[†,⊥] Peng Liu,[‡] Dasheng Leow,[§] Tian-Yu Sun,[†] Ping Chen,[†] Xinhao Zhang,[†] Jin-Quan Yu,*[,§] Yun-Dong Wu,*[,†,‖] and K. N. Houk*[,‡]

[†]Laboratory of Computational Chemistry and Drug Design and Laboratory of Chemical Genomics, Peking University Shenzhen Graduate School, Shenzhen 518055, China

[‡]Department of Chemistry and Biochemistry, University of California, Los Angeles, California 90095, United States

[§]Department of Chemistry, The Scripps Research Institute, 10550 North Torrey Pines Road, La Jolla, California 92037, United States

[‖]College of Chemistry and Molecular Engineering, Peking University, Beijing 100871, China

S *Supporting Information*

ABSTRACT: Density functional theory investigations have elucidated the mechanism and origins of *meta*-regioselectivity of Pd(II)-catalyzed C−H olefinations of toluene derivatives that employ a nitrile-containing template. The reaction proceeds through four major steps: C−H activation, alkene insertion, β-hydride elimination, and reductive elimination. The C−H activation step, which proceeds via a concerted metalation−deprotonation (CMD) pathway, is found to be the rate- and regioselectivity-determining step. For the crucial C−H activation, four possible active catalytic species—monomeric $Pd(OAc)_2$, dimeric $Pd_2(OAc)_4$, heterodimeric $PdAg(OAc)_3$, and trimeric $Pd_3(OAc)_6$—have been investigated. The computations indicated that the C−H activation with the nitrile-containing template occurs via a Pd−Ag heterodimeric transition state. The nitrile directing group coordinates with Ag while the Pd is placed adjacent to the *meta*-C−H bond in the transition state, leading to the observed high *meta*-selectivity. The $Pd_2(OAc)_4$ dimeric mechanism also leads to the *meta*-C−H activation product but with higher activation energies than the Pd−Ag heterodimeric mechanism. The Pd monomeric and trimeric mechanisms require much higher activation free energies and are predicted to give *ortho* products. Structural and distortion energy analysis of the transition states revealed significant effects of distortions of the template on mechanism and regioselectivity, which provided hints for further developments of new templates.
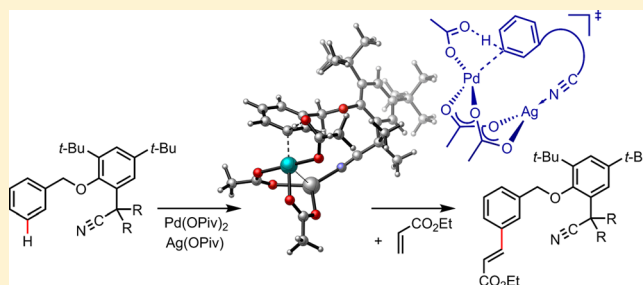
1. INTRODUCTION

Transition-metal-catalyzed functionalization of the C−H bond is emerging as a very powerful methodology for C−C bond formation and has received great attention in recent years.[1] Direct C−H activation and functionalization bypasses preparation of the prerequisite activated coupling partner in traditional cross-coupling reactions. Efficient and highly selective C−H functionalizations will undoubtedly have wide applications in the synthesis of natural products, pharmaceuticals, and agrochemicals. Functionalization of *ortho* arene C−H bonds can be achieved by σ-chelation-directed metalation with directing groups such as pyridines, amides, oximes, acetanilides, and triazene.[2] Considerable recent progresses of metal-catalyzed *para*-selective C−H functionalization reactions have been accomplished.[3] Recently, extensive and innovative efforts toward *meta*-selective C−H functionalizations have been reported.[4] However, controlling site selectivity, especially *meta*-selective functionalization of electron-rich aromatic rings, is still one of the greatest challenges in this active research field.

A new approach to control the site-selectivity in C−H activations was recently reported by Yu and co-workers:[4f] easily removable nitrile-containing templates direct the activation of *meta*-C−H bonds of electron-rich monosubstituted arenes (Scheme 1a). The novel templates override the electronic preferences and selectively activate the distal *meta*-C−H bonds. The mechanism of these transformations and, more importantly, the origins of *meta*-selectivity are still unknown. This dramatically hindered the development of this template-directed methodology for other aromatic or heteroaromatic systems. Another key challenge for template design is to understand the effects of template length and of bulky *t*-Bu and *i*-Bu substituents on reactivity and *meta*-selectivity. The special benzyl ether linker in the template is considerably longer than the commonly used directing groups in *ortho*-C−H bond activations.[2] Bulky substituents at some critical positions of the

Scheme 1. (a) Palladium-Catalyzed, Template-Directed *Meta*-Selective C−H Olefination of Toluene Derivatives[4f] and (b) Active Catalytic Species Considered by Computations

(a)

R = *i*Bu; 63% yield, *m*:*p*:*o* = 95:4:1
R = Me; 60% yield, *m*:*p*:*o* = 91:7:2

substrate used in computations
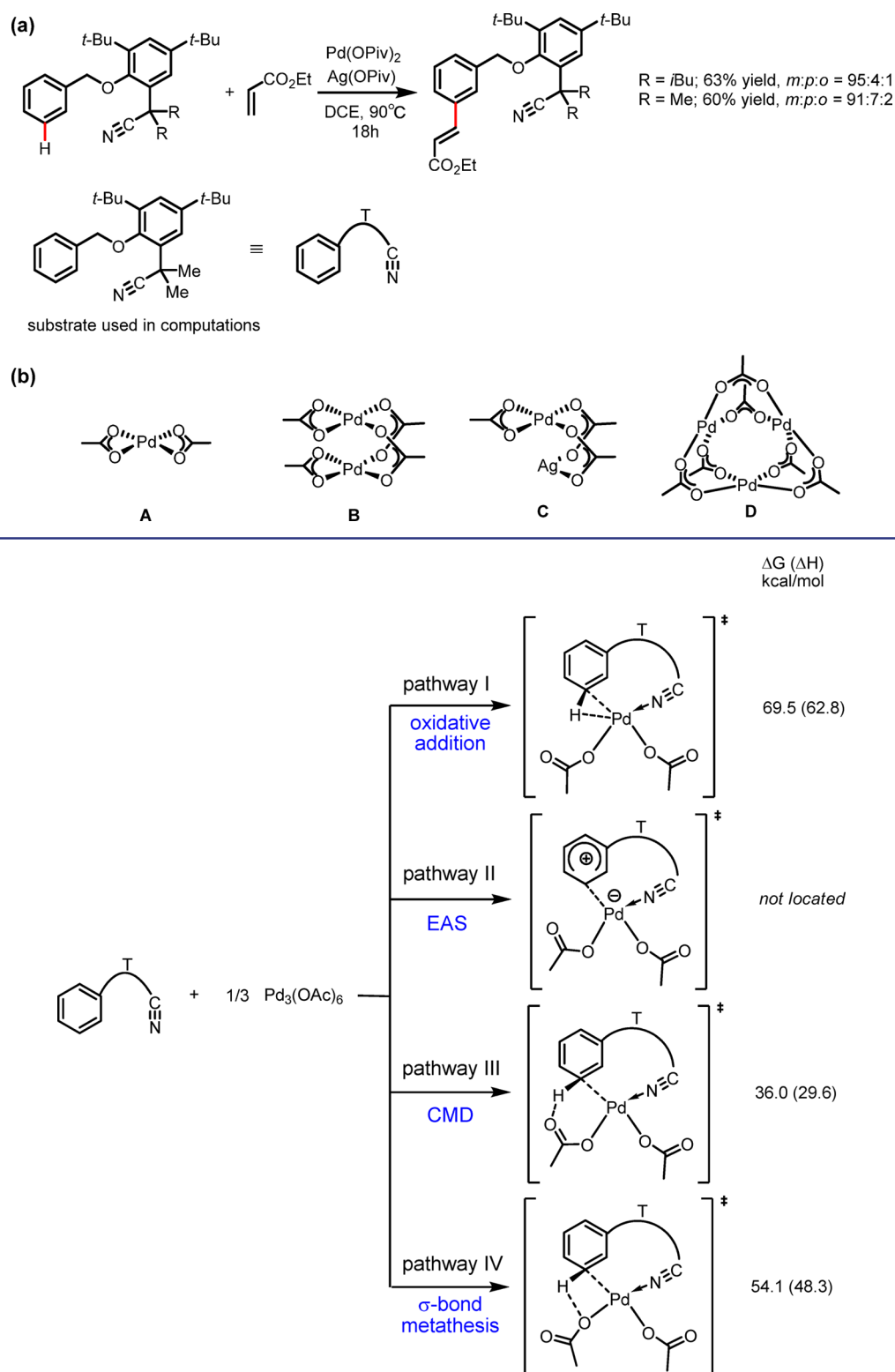
(b)

A   B   C   D

Figure 1. Monomeric C−H activation pathways and computed activation energies.

template are essential for reactivity and *meta*-selectivity, presumably to control the flexibility of the linker[5] and to predistort the template into a transition-state-like conformation. Detailed analysis of these possible effects necessitates a thorough computational investigation. Intrigued by this new

experimental strategy to activate remote *meta*-C−H bonds, we have conducted computational studies to elucidate the mechanism and origins of the *meta*-selectivity of this palladium-catalyzed template-directed *meta*-selective C−H olefination of toluene derivatives.

Scheme 2. Catalytic Cycle of Pd Monomeric Mechanism
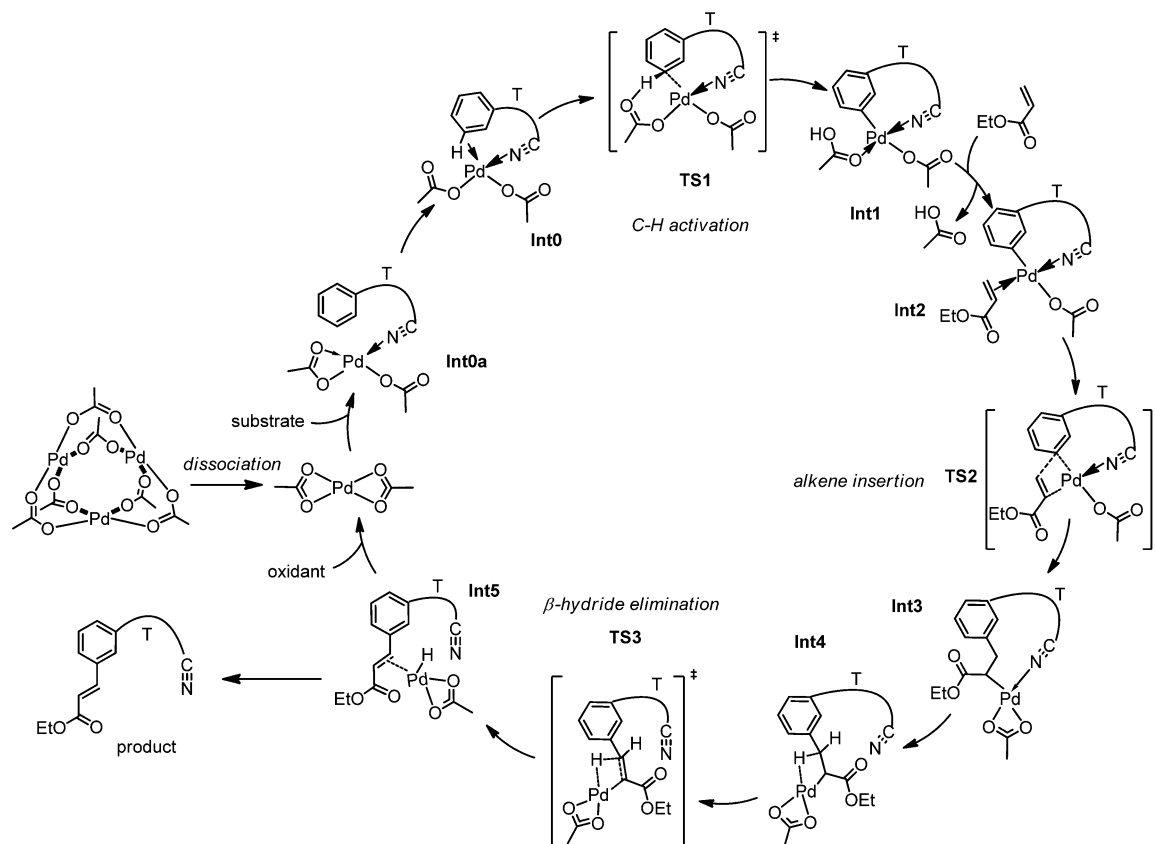
Palladium catalysts can be effective in various forms depending on the ligand, temperature, solvent, and other reaction conditions.[6] Although the general mechanism of Pd-catalyzed C–H bond activation has been thoroughly investigated by both computations[7] and experiments,[8] there have been active debates on whether the monomeric, dimeric, or trimeric Pd is the active catalyst in C–H activations and related transformations. In oxazoline-directed, Pd(II)-catalyzed sp[3] C–H bond iodination, the X-ray structure of the C–H activated trinuclear palladacycle intermediate was obtained.[9,10] Our computational study indicated that this trimeric intermediate is formed via a monomeric Pd transition state.[9] Acetate-bridged Pd[II]–Pd[II] dimer structures are common, for example, [(2-phenylpyridine)Pd(μ-OAc)]₂, and there is no Pd–Pd bonding interaction in these compounds.[11] High-valent binuclear Pd[III]–Pd[III] complexes have also been developed to serve as redox catalysts for C–X reductive elimination.[12] It was reported recently by Hartwig and co-workers[13] that C–H arylation of pyridine N-oxide is mediated by a cyclopalladated dinuclear Pd complex in which C–H activation occurs at one Pd center and the activated complex transfers to the second Pd center to undergo functionalization. Both monometallic and bimetallic reaction pathways were considered in the study by Sanford and Schoenebeck and co-workers[14] of palladium-mediated C–H oxidative coupling of 1,3-dimethoxybenzene with benzo[h]quinolone. They clarified the role of anionic ligands in the site selectivity and showed that the selectivity predicted is equivalent for carbonate and acetate, regardless of whether dinuclear or mononuclear Pd complexes are considered. For such Pd[II]–Pd[II] dimer structures, C–H activation of the substrate occurs at one Pd[II] center. We speculated the active catalyst species may be affected by the template. Therefore, in this study, we investigated several possible C–H activation mechanisms involving monomeric, dimeric, and trimeric Pd complexes and a heteronuclear Pd–Ag complex as the active catalyst, as shown in Scheme 1b.

2. COMPUTATIONAL DETAILS

All calculations were carried out with the Gaussian 09 package.[15] Geometry optimizations were performed with B3LYP.[16] LANL2DZ + f (1.472) basis set with effective core potential (ECP) was used for Pd, LANL2DZ + f (1.611) basis set[17] with ECP was used for Ag, and the 6-31G (d) basis set[18] was used for other atoms. Frequency analysis was conducted at the same level of theory to verify the stationary points to be minima or saddle points and to obtain zero-point energy (ZPE) and thermal energy corrections at 363.15 K. Single-point energies were calculated with M06[19]/SDD[20]-6-311++G(d,p),[21] which is generally considered to be more accurate for energetics. Selected key model structures were also evaluated with MP2[22]/SDD-6-311++G(d,p) and CCSD(T)[23]/SDD-6-31G(d). The MP2 and CCSD(T) calculations are consistent with the M06 results (see Supporting Information for details). Furthermore, a similar level of method was reported to have demonstrated satisfactory performance in our previous study on Pd-catalyzed C–H activations.[9] Single-point solvation energies were calculated by using SMD solvation model (solvent = 1,2-dichloroethane).[24] Computed structures are illustrated using CYLView.[25]
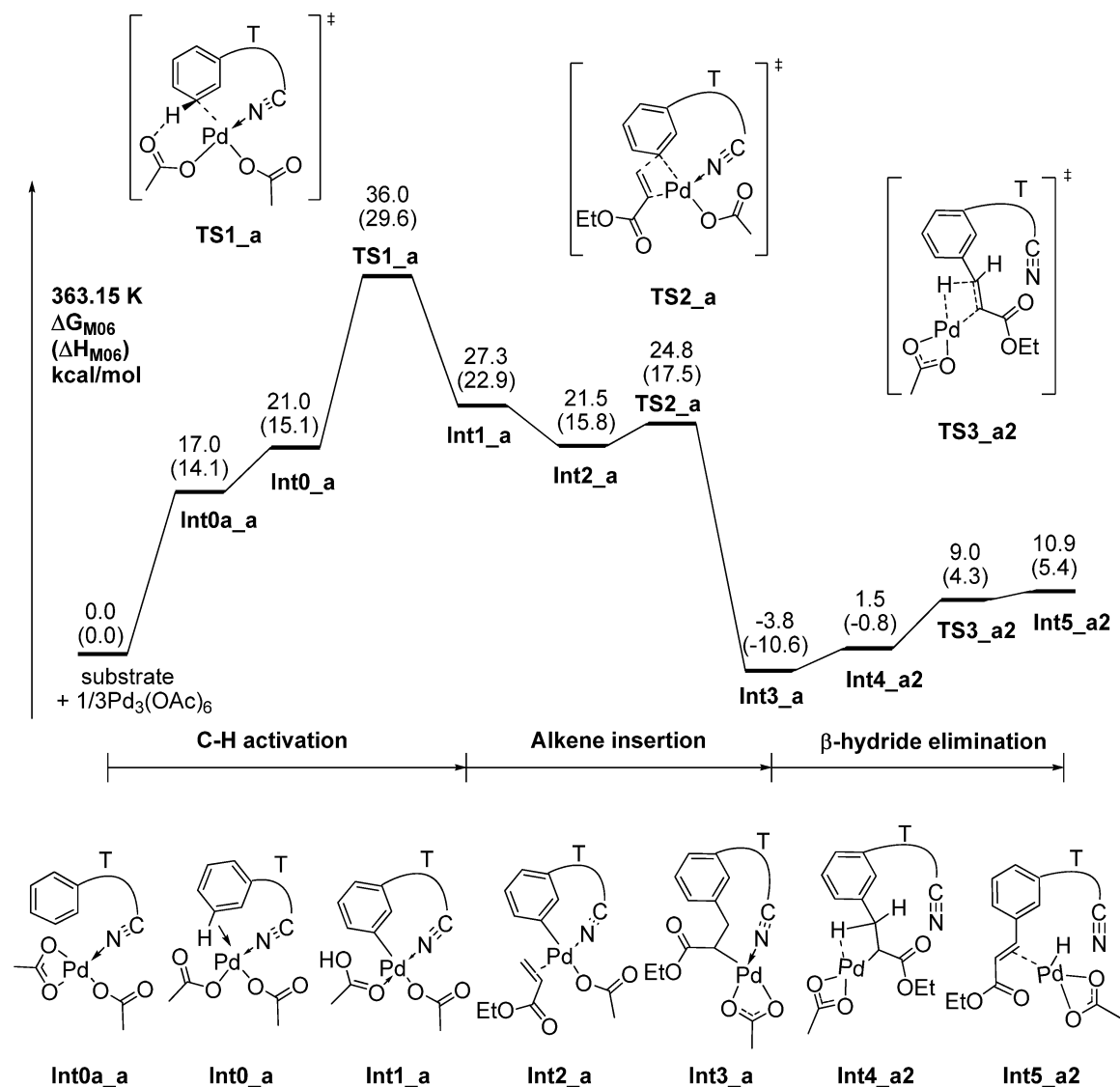
Figure 2. M06 free energy profile for the *meta* pathway in the monomeric Pd(OAc)$_2$ mechanism. Enthalpies are given in parentheses.

3. RESULTS AND DISCUSSION

3.1. Pd(OAc)$_2$ Monomeric Mechanism. Four C−H activation pathways involving the mononuclear Pd(OAc)$_2$ catalyst have been investigated with computations (Figure 1): oxidative addition of the C−H bond (pathway I), electrophilic aromatic substitution (EAS) (pathway II), concerted metalation−deprotonation (CMD) (pathway III),[26] and σ-bond metathesis (pathway IV). The computed activation free energies and enthalpies of the C−H activation transition states are shown in Figure 1. These energies are with respect to the resting state, Pd$_3$(OAc)$_6$ trimer, which is consistent with our previous study.[9] The geminal *i*-Bu groups were replaced with methyl groups in the calculations (Scheme 1a, R = Me).[27] Although Pd(OPiv)$_2$ and Ag(OPiv) were found superior to Pd(OAc)$_2$ and Ag(OAc) in the experiment, the acetates were used in the calculations to save computation time.

Pathway III (CMD) was found to be the most favorable among the four pathways.[28] This agrees with previous explorations of palladium(II) acetate-catalyzed C−H activation reactions that also predict CMD is the dominant mechanism.[26] The catalytic cycle and the complete free energy profile of the Pd monomeric mechanism are presented in Scheme 2 and

Figure 2. At the outset of the catalytic cycle, the trimeric palladium acetate dissociates into a monomer. The first key step is the CMD C−H activation, in which the bound acetate acts as a base to deprotonate the arene (**TS1_a**), while a new Pd−C bond is formed. The C−H activation step leads to a monomeric palladacycle intermediate **Int1_a**. The second key step is alkene insertion (**TS2_a**) involving the olefin-coordinated palladacycle intermediate **Int2_a** to form **Int3_a**. The third step is β-hydride elimination (**TS3_a2**), as the weakly coordinated nitrile group dissociates and the hydride is transferred to Pd to form the product π-complex **Int5_a2**. In the last few steps of the catalytic cycle, the palladium hydride intermediate **Int5_a2** undergoes product dissociation, reductive elimination to release the acetic acid, and oxidation of Pd^0 with the Ag^I oxidant to regenerate the Pd^{II} catalyst. There are several possibilities with the different orders of these steps. This process is expected to be highly exergonic and require low activation barriers.[4e,29] The details of these steps were not calculated.

As shown in Figure 2, the rate-determining step for the *meta* pathway in the monomeric Pd(OAc)$_2$ CMD mechanism is the C−H activation step, with activation free energy of 36.0 kcal/mol with respect to the catalyst resting state, trimeric
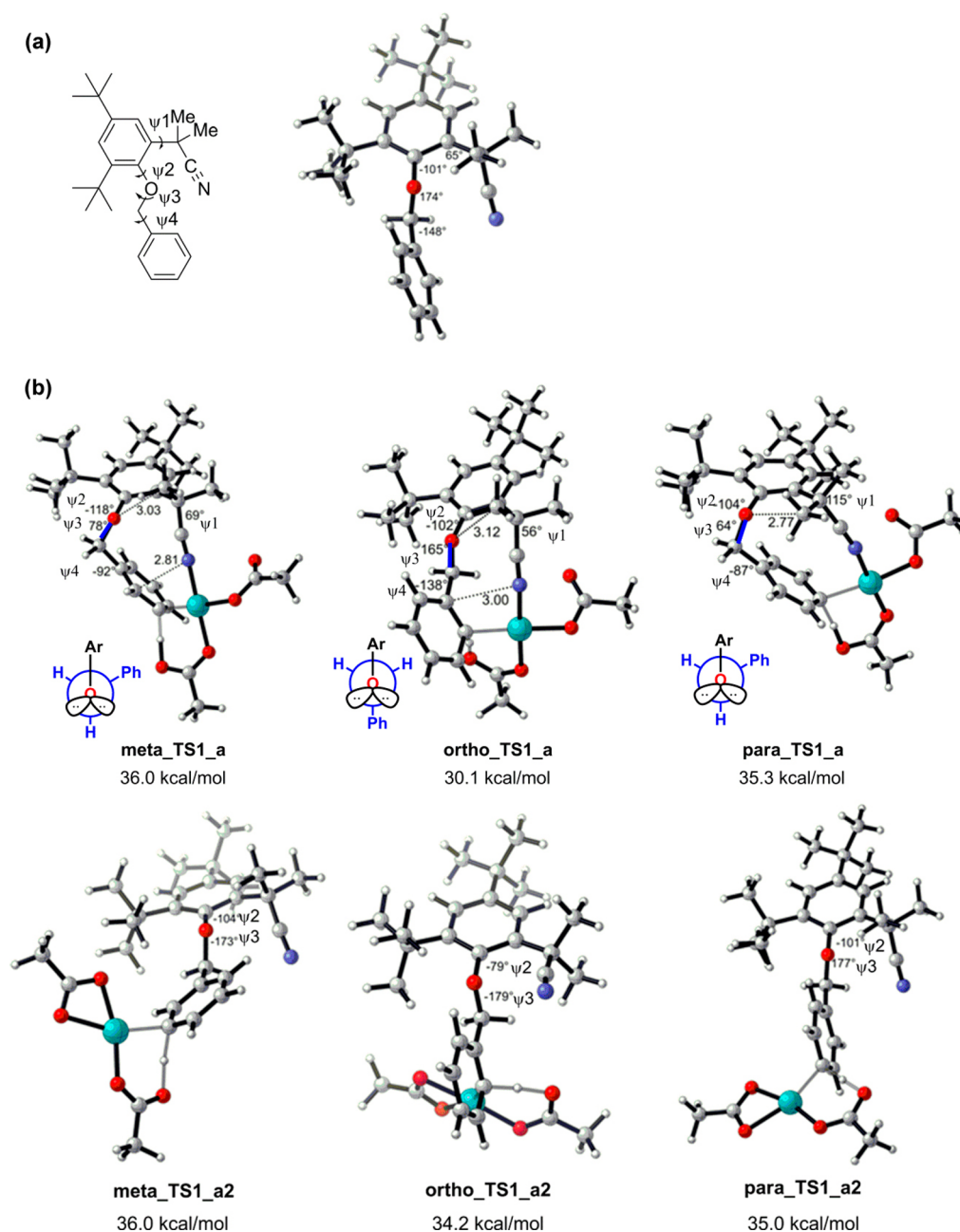
Figure 3. (a) Lowest energy conformation of toluene derivative substrate with nitrile-containing template. (b) Optimized geometries of *meta, ortho,* and *para* C−H activation transition states of the monomeric Pd(OAc)$_2$ mechanism. In **TS1_a**, the nitrile group is coordinated to Pd; in **TS1_a2**, it is not. Gibbs activation free energies with solvation correction are given in kilocalories per mole.

Pd$_3$(OAc)$_6$, plus the separate substrate. Since the regioselectivity is determined by the transition state (TS) of C−H activation, **TS1**, the regioisomeric transition states for this step were investigated to understand the selectivity. Regarding site selectivity and nitrile-directing effect in the Pd monomeric mechanism, six isomeric TS structures for the C−H activation step were computed: three transition states with nitrile coordinated to Pd (**meta_TS1_a, ortho_TS1_a,** and **para_-TS1_a**) and three transition states without nitrile coordination (**meta_TS1_a2, ortho_TS1_a2,** and **para_TS1_a2**). These structures are shown in Figure 3b.

In the monomeric TS structures without nitrile coordination (**meta_TS1_a2, ortho_TS1_a2,** and **para_TS1_a2**), the template adopts a similar conformation as in the reactant

(Figure 3a). The dihedral angles of the benzyl ether C−O bond $\psi3$ in these uncoordinated transition states and in the reactant are all close to 180° (Figure 3). The selectivity is governed by the electronic effects that preferentially activate the *ortho*-C−H bond of the electron-rich arene. The *ortho* TS (**ortho_TS_a2**) is favored over the corresponding *meta* and *para* TS structures (**meta_TS1_a2** and **para_TS1_a2**) by 1.8 and 0.8 kcal/mol, respectively. This indicates the *ortho*- and *para*-C−H bonds are intrinsically preferred in the absence of the nitrile directing group. Coordination of nitrile leads to comparable activation free energy barriers for the *meta* and *para* pathways while, to our surprise, it dramatically stabilizes the *ortho* TS (**ortho_T-S1_a**), which is now 5.9 kcal/mol more stable than the *meta* TS (**meta_TS1_a**). This suggests that the template actually

Scheme 3. Conformations of *Meta*-C–H Bond Activation Transition State Involving Dimeric Pd Catalyst[a]
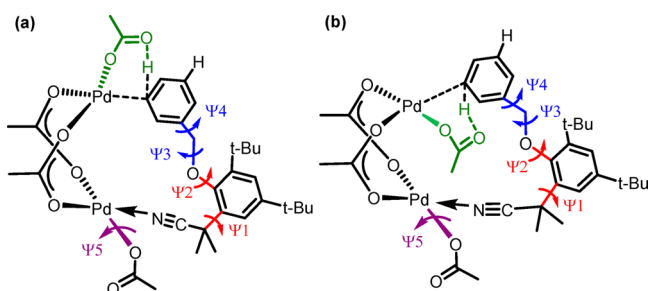
[a] (a) Two acetate groups (green and purple) are on different sides. (b) Two acetate groups are positioned on the same side.

promotes *ortho*-C–H activation if the reaction occurs via the monomeric Pd mechanism.

Analysis of distortion of the template in the nitrile-coordinated macrocyclic transition states indicates dramatic differences in the conformation and strain energy of the template in the *ortho*, *meta*, and *para* pathways. Distortion/interaction energy analysis of the monomeric transition states indicates that the origin of differences between activation energies in the *ortho*, *meta*, and *para* transition states is the same as the differences of distortion energies of the substrate in the transition states (36.7, 44.1, and 43.2 kcal/mol for **ortho_TS1_a**, **meta_TS1_a**, and **para_TS1_a**, respectively; see Supporting Information for more details). The greater ring strain in **meta_TS1_a** and **para_TS1_a** is mostly caused by torsion about the benzyl ether C–O bond, which places two bulky groups in gauche position in the *meta* and *para* TS ($\psi3 = 78°$ and $64°$, respectively), while they are anti in the preferred *ortho* TS ($\psi3 = 165°$). In addition, **meta_TS1_a** is also destabilized by torsion about $\psi2$ ($-118°$ vs $-101°$ in the reactant) as well as repulsions between the nitrile nitrogen atom and the *ortho* carbon atom (2.81 Å). **para_TS1_a** is also destabilized by steric repulsions between the ether oxygen and methyl group (O–C distance of 2.77 Å). In summary, the monomeric mechanism cannot explain the *meta*-regioselectivity observed experimentally (*m:p:o* = 91:7:2). The *meta* pathway leads to greater distortion of the nitrile-containing template when bound to a monomeric Pd catalyst.

3.2. Pd$_2$(OAc)$_4$ Dimeric Mechanism. It is surmised that, with a long tether, the nitrile on the template could bind to one Pd in the dimeric Pd$_2$(OAc)$_4$ complex while the arene C–H bond is placed adjacent to another Pd to undergo C–H activation. The computational results for the monomeric mechanism hinted that such a dimeric activation mode may relieve the ring strain of the *meta* TS by forming a larger macrocycle. Therefore, the dimeric Pd mechanism was investigated computationally.
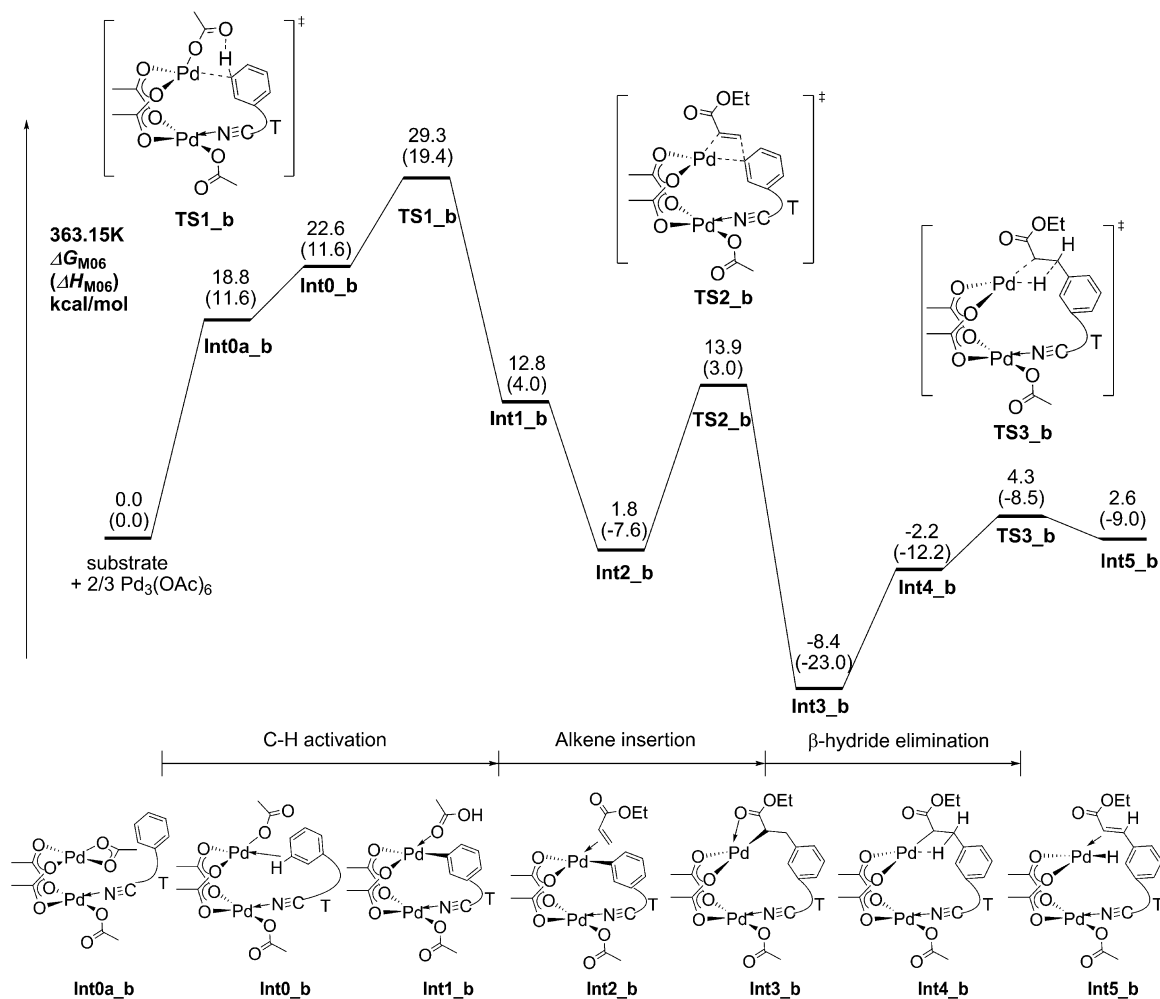

Figure 4. M06 free energy profile for the *meta* pathway in the dimeric Pd$_2$(OAc)$_4$ mechanism. Enthalpies are given in parentheses.
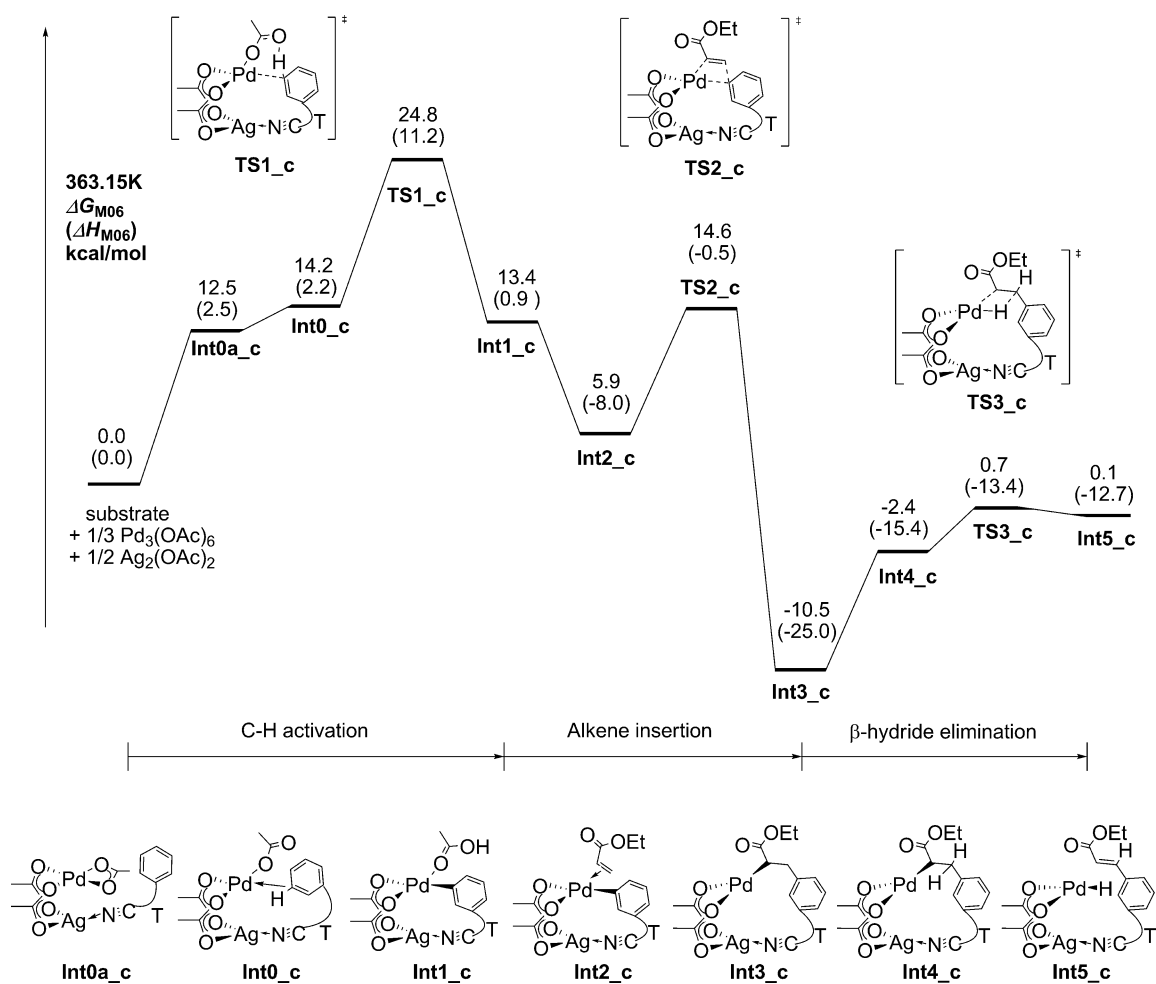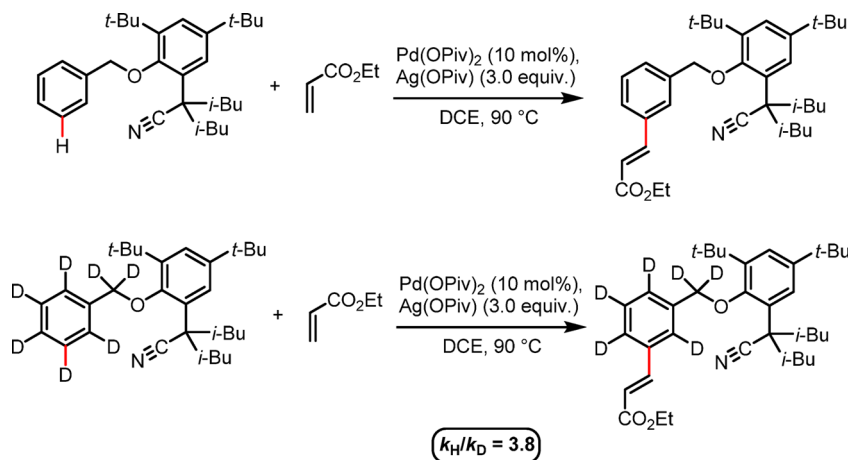
Figure 5. M06 free energy profile for *meta* pathway in heterodimeric PdAg(OAc)$_3$ mechanism. Enthalpies are given in parentheses. All energies are with respect to Pd$_3$(OAc)$_6$ and Ag$_2$(OAc)$_2$.[35]

Scheme 4. Kinetic Isotope Effects in C—H Olefination

$k_H/k_D = 3.8$

In the dimeric Pd mechanism, there are many possible conformations for the transition states since they are macrocyclic 14- (*ortho*), 15- (*meta*), or 16- (*para*) membered rings. We have performed a systematic search for all the TS conformers. Four major factors were considered in a systematic conformational search. As shown in Scheme 3, the first factor is the dihedral angles $\psi 1$ and $\psi 2$, which determine the relative orientations of nitrile group and the substrate benzene ring (on

the same side of the template benzene ring or on different sides). The second factor is the dihedral angles $\psi 3$ and $\psi 4$ that determine which of two *meta* C—H bonds (or two *ortho* C—H bonds) will be activated. The third factor is the rotation of the spectator acetate group (dihedral angle $\psi 5$), which brings the carbonyl above or below the coordination plane of palladium. The fourth factor is the relative position of the nitrile coordination site and the C—H bond activation site. The

Scheme 5. Monomeric and Dimeric C−H Activation Transition States

ortho-selective

meta-selective
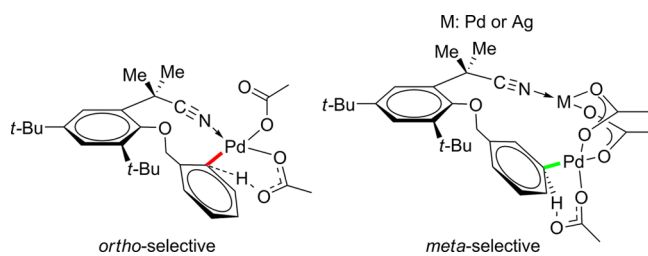
activated C−H bond can be directly above the nitrile coordination site on the other Pd center (Scheme 3b) or at the cis-position (Scheme 3a). In total, 43 conformers of the C−H activation transition states[30] were located.

Based on the most stable TS conformers, the free energy profile of the dimeric Pd mechanism is shown in Figure 4. The

Table 1. Distortion Energy Analysis of C−H Activation Transition States of PdAg(OAc)$_3$ Mechanism

distortion energy	meta_TS1_c	ortho_TS1_c	para_TS1_c
E_{cat} (kcal/mol)	35.2	36.3	36.3
E_{sub} (kcal/mol)	33.3	37.7	35.6
E_{total} (kcal/mol)	68.5	74.0	71.9

C−H bond activation step is also the rate- and regioselectivity-determining step in this mechanism. The 3D structures of the C−H activation transition states are shown in Figure 6. The C−H activation barrier is 29.3 kcal/mol (**meta_TS1_b**), significantly lower than that for the monomeric mechanism [$\Delta G^{\ddagger}(meta)$ = 36.0 kcal/mol], with respect to the same Pd$_3$(OAc)$_6$ catalyst precursor. Direct comparison of the activation energies of monomeric and dimeric Pd pathways requires correct treatment of several key interactions, including nonbonding Pd−Pd interactions, dispersion energies in the

meta_TS1_b

29.3 kcal/mol

ortho_TS1_b

29.7 kcal/mol

para_TS1_b

33.4 kcal/mol

meta_TS1_c

24.8 kcal/mol

ortho_TS1_c

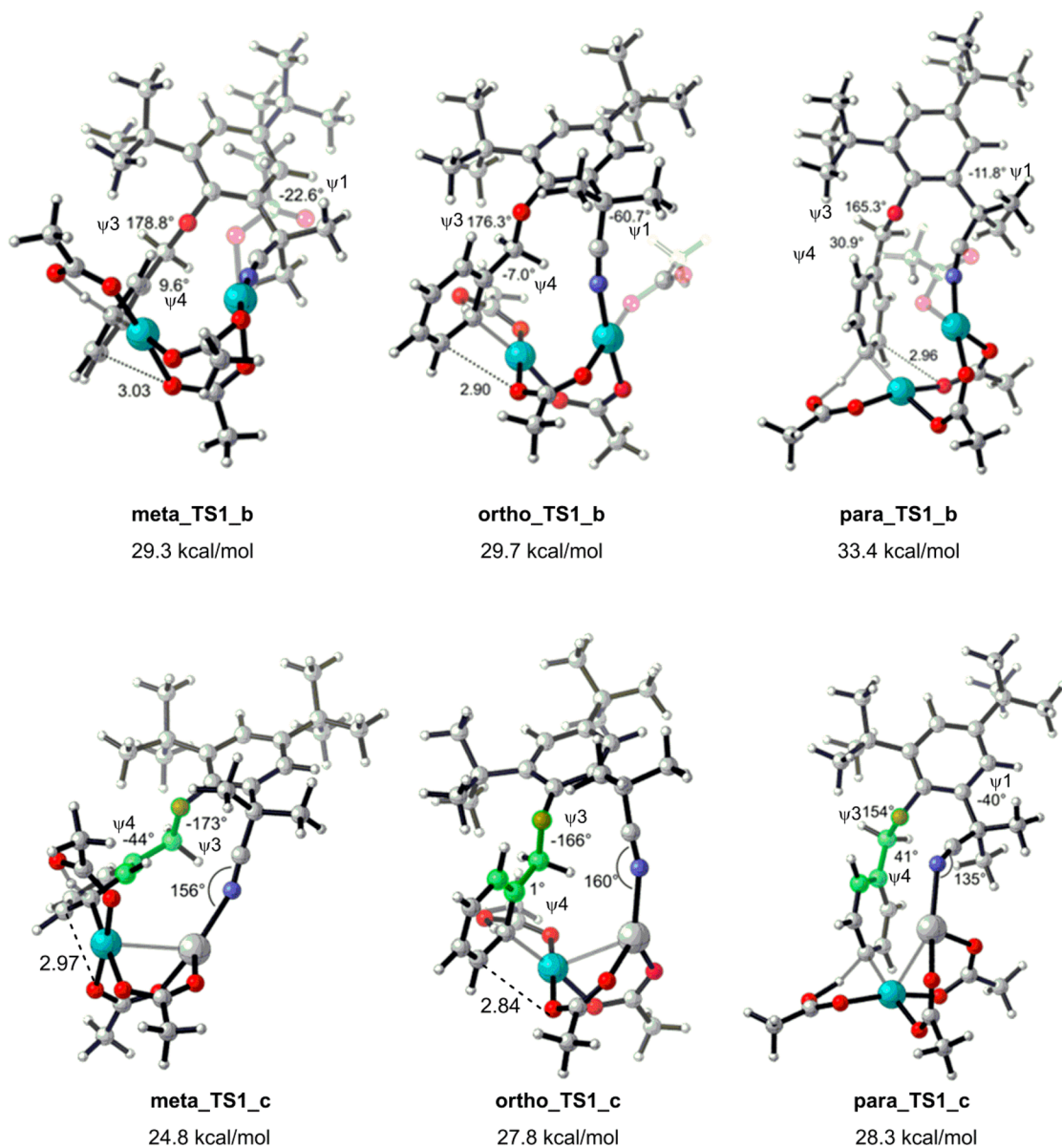27.8 kcal/mol

para_TS1_c

28.3 kcal/mol

Figure 6. C−H activation transition states and activation free energies for *meta, ortho*, and *para* pathways of Pd−Pd (**TS1_b**) and Pd−Ag (**TS1_c**) dimeric mechanisms.

macrocyclic TS, and ligand binding energies. Recent benchmark studies indicated that the computational method used in this study (M06 with a large basis set) is expected to provide reasonable accuracy to describe the ligand binding energies and dispersion interactions in the monomeric and dimeric transition-state complexes.[31] We have tested the performance of M06 in describing the dimerization energy of Pd dimer with MP2 and CCSD(T). M06 gave reasonable agreement with these higher-level calculations (see Supporting Information), suggesting it is also applicable to describe the nonbonding Pd–Pd interactions in the current dimeric Pd system.

There exist many similar energy conformers for these macrocyclic transition states (eight conformations were found within 2 kcal/mol from the lowest energy conformer; their structures and corresponding energies are presented in Supporting Information). The computed activation free energies for the lowest energy conformers of the *meta*, *ortho*, and *para* C–H activation pathways are 29.3, 29.7, and 33.4 kcal/mol, respectively, all significantly lower than for the monomeric pathways. The **meta_TS1_b** has the lowest activation energy. It is worth noting that, for the Pd$_2$(OAc)$_4$ dimeric mechanism, seven low-energy TS conformers contribute to the *meta*-C–H bond activation (energy differences within 2 kcal/mol), while only one low-energy TS conformer is responsible for *ortho*-C–H bond activation among these eight most stable TS conformers. Other *ortho* TS conformers are all at least 2 kcal/mol less stable than the lowest energy conformer. The Boltzmann distribution of these TS conformers indicates that the *meta* pathway is more favorable than the *ortho* pathway with a *meta:ortho* product ratio of 73:27 at 90 °C. This is in agreement with the *meta*-selectivity in the experiment, although the computed ratio is slightly lower. We will discuss the structures of the regioisomeric transition states and the distortions of the tethered template in more detail later.

3.3. PdAg(OAc)$_3$ Heterodimeric Mechanism. In the experiment, more than 2.5 equiv of Ag(OPiv) is found to be a crucial additive for this Pd(II)-catalyzed olefination of toluene derivatives with the nitrile-containing template. Replacing Ag with other oxidants leads to very low yield and diminishes the *meta*-selectivity. Similar effects of Ag were also found in a related Pd-catalyzed C–H activation containing a nitrile group.[32] Given the usage of excess Ag salt, we envisaged that Ag$^+$ could play a dual role in this reaction. Besides acting as an oxidant to effectively turn over the catalytic cycle, it may replace one of the Pd centers in the dimeric TS and coordinate with the nitrile. In the PdAg(OAc)$_3$ heterodimeric complex with the substrate (**Int0a_c**), the two bridging acetate groups are cis-coordinated to the Ag. This creates a vacant coordination site to allow the Ag to bind efficiently to the nitrile on the template. Since Ag(I) is isoelectronic with Pd(II), such a heterodimeric Pd–Ag complex is structurally similar to the Pd–Pd dimeric complex, except that the Ag is three-coordinated. Similar Pd–Ag bimetallic complexes with three- or four-coordinated Ag have been identified by X-ray crystallography.[33] Although heterodinuclear catalytic systems have been proposed in various scenarios,[34] C–H activation involving a Pd–Ag bimetallic catalyst has not been reported in the literature. We explored the activation energies and regioselectivities involving the hetero-dimeric Pd–Ag complex as the active catalyst.

The free energy profile for the *meta* pathway in the heterodimeric PdAg(OAc)$_3$ mechanism is shown in Figure 5. Again, the C–H bond activation step is the rate- and regioselectivity-determining step. The most stable transition states for *meta*-, *ortho*-, and *para*-C–H activation are **meta_TS1_c** (24.8 kcal/mol), **ortho_TS1_c** (27.8 kcal/mol), and **para_TS1_c** (28.3 kcal/mol), respectively. The 3D structures of these C–H activation transition states are shown in Figure 6. These calculated free energy barriers are lower than those for the aforementioned monomeric and dimeric Pd mechanisms and indicate the reaction is facile under the experimental conditions (90 °C). Similar to the Pd dimeric mechanism, these transition states are also stabilized by Ag–nitrile coordination. The transition states in which the silver is not coordinated to the nitrile, **meta_TS1_c2**, **ortho_TS1_c2**, and **para_TS1_c2**, are much less stable at 36.2, 32.8, and 34.7 kcal/mol, respectively (Supporting Information). This demonstrates the strong nitrile directing effects in the bimetallic Pd–Ag mechanism, facilitated by the vacant binding site of the Ag center anti to the bridging acetates. The *meta*-C–H bond activation is also preferred in the Pd–Ag mechanism, in agreement with the experiment. Detailed analysis on regioselectivity will be discussed later.

Kinetic isotope effects (KIE) were also studied experimentally and theoretically. The experimental k_H/k_D is 3.8 (Scheme 4). Our computed KIE results for Pd monomeric mechanism **meta_TS1_a**, Pd dimeric mechanism **meta_TS1_b**, and Pd–Ag dimeric mechanism **meta_TS1_c** are 3.6, 4.1, and 3.8, respectively. In these calculations, the geminal *i*-Bu groups α to the nitrile were replaced with Me groups, as in the rest of the calculations (see above). We also calculated the KIE values with the real experimental substrate with geminal *i*-Bu groups. The results are almost identical to those for Me-substituted substrate (3.6, 4.1, and 3.9, for monomeric Pd, dimeric Pd–Pd, and Pd–Ag mechanisms, respectively). These computed KIEs for three different mechanisms are all consistent with the experimental values. It is understandable since the active sites for the CMD processes in all three mechanisms are similar. Unfortunately, comparison with the experimental KIE cannot provide further evidence to differentiate the above three mechanisms.

3.4. Pd$_3$(OAc)$_6$ Trimeric Mechanism. Since the dimeric Pd–Pd and Pd–Ag mechanisms have lower barriers than the monomeric Pd mechanism and can successfully explain the *meta*-selectivity, we further investigated whether the trimeric form of the Pd catalyst is also reactive in the C–H activation. Similar to the dimeric case, the macrocyclic C–H activation transition state involving the trimeric Pd catalyst has many possible conformations. Due to greater distortions of the trimeric catalyst, the lowest activation energy of the trimeric transition states is 37.9 kcal/mol. This ruled out the trimeric mechanism in this reaction (see Supporting Information for more details).

3.5. Origins of *Meta*-Selectivity in Dimeric Mechanism. The explorations of the four different reaction mechanisms suggest that the trimeric mechanism can be excluded due to its highest energy barrier. The monomeric mechanism requires a higher barrier than the two dimeric mechanisms and is *ortho*-selective, which does not agree with the observed *meta*-selectivity. The dimeric Pd–Pd and Pd–Ag mechanisms have lower activation barriers than the trimeric and monomeric mechanisms and are both *meta*-selective (Scheme 5). Why do the monomeric and dimeric pathways promote different C–H activation sites?

The calculated regioselectivities shown above indicate that, in the monomeric Pd pathway, the Pd center activates the *ortho* position more favorably. Forcing the Pd to reach the *meta*

position will induce greater ring strain when adjusting the conformation of the substrate in the monomeric TS. While in the dimeric transition states, the nitrile and the activated C−H bond are bound to different Pd atoms. This extends the ring size of the macrocyclic TS and places the Pd near the *meta*-C−H bond without increasing ring strain. The *meta* TS is also more flexible than the *ortho* TS. Several low-energy *meta* TS isomers were found in the conformational search.

Geometries of the most stable transition states involving Pd−Pd and Pd−Ag dimeric catalysts are shown in Figure 6. Given the similarity between the TS geometries in the two mechanisms, we will only discuss the geometrical analysis of the Pd−Ag transition states (**TS1_c**) to explain the origins of *meta*-selectivity.

The **meta_TS1_c** is the most stable transition structure among these transition states. The *ortho* TS (**ortho_TS1_c**) is 3.0 kcal/mol less stable than **meta_TS1_c**. In contrast to the monomeric transition states, in which the *meta*- and *para* TS are destabilized by the gauche conformation about the benzyl ether bond ($\psi 3$), no torsional strain about $\psi 3$ is observed in the dimeric transition states. The larger ring size in the dimeric TS allows the anti arrangement about $\psi 3$ in all three regioisomeric transition states ($\psi 3 = -173°, -166°$, and $154°$ for *meta, ortho*, and *para* TS, respectively). Compared to **meta_TS1_c**, the *ortho* TS is destabilized by the planar conformation of the reacting benzene ring ($\psi 4 = 1°$), which induces repulsions with the ether oxygen. Furthermore, the distance between the oxygen of the bridged acetate cis to the Pd−C bond and the carbon adjacent to the activated C−H bond is 2.97 Å for **meta_TS1_c** and 2.84 Å for **ortho_TS1_c**, indicating stronger repulsions in the *ortho* TS. The *para* TS (**para_TS1_c**) is destabilized by the unfavorable binding angle of the nitrile to Ag. The C−N−Ag angle is about 160° in both **meta_TS1_c** and **ortho_TS1_c**, close to the optimum nitrile ligand binding angle of 180°, while this angle is distorted to 135° in **para_TS1_c**.

To further cast light on how these different factors control the regioselectivity, a distortion/interaction analysis[36,7f] was performed for the dimeric Pd−Ag mechanism. The distortion of the *meta* structure is the smallest among these TS structures. As shown in Table 1, while the distortion of the $PdAg(OAc)_3$ catalyst is similar, the substrate distortions are dramatically different in the three TS structures. The distortion energies of the substrate in **ortho_TS1_c** and **para_TS1_c** are 5.5 and 3.4 kcal/mol higher than that in **meta_TS1_c**, respectively. These results again demonstrate that distortion of substrate in the C−H activation transition states controls the site selectivity.

The computational studies on selectivity show that the dimeric mechanisms enable the Pd center to interact with the *meta* position favorably, since they have longer intrinsic lengths than monomeric Pd complexes. The novel dimeric mechanisms successfully explain the puzzling *meta*-selectivity found experimentally.

4. CONCLUSIONS

We have investigated the mechanism and origins of *meta*-selectivity in Pd-catalyzed C−H activation with a nitrile-containing template (Scheme 1a). We compared the activation energies and predicted selectivities of multiple C−H activation mechanisms involving monomeric Pd, dimeric Pd−Pd and Pd−Ag, and trimeric Pd complexes as the active species. In all pathways investigated, the nitrile on the template preferentially coordinates to the Pd or Ag center. The computations indicated the Pd-catalyzed C−H activation occurs via a concerted metalation−deprotonation (CMD) mechanism involving dimeric catalytic species. The homodimeric $Pd_2(OAc)_4$ and heterodimeric $PdAg(OAc)_3$ mechanisms both require lower activation barriers for C−H activation than the monomeric and trimeric mechanisms. This is due to less ring strain in the macrocyclic nitrile-coordinated C−H activation transition states in the dimeric mechanisms. Both $Pd_2(OAc)_4$ and $PdAg(OAc)_3$ dimeric mechanisms selectively activate the *meta*-C−H bond, in agreement with experiment. In contrast, the monomeric Pd mechanism is *ortho*-selective. These computational results strongly support the dimeric mechanisms involving either $Pd_2(OAc)_4$ or $PdAg(OAc)_3$ as the active species in C−H functionalization with the nitrile-containing template. Our computational results also demonstrate the dual role of AgOAc functioning as both an oxidant and part of the heteronuclear active species in the mechanism involving $PdAg(OAc)_3$. The preference for the dimeric pathway is apparently attributed to the unique structure of the template in this study. We expect this preference may alter when other templates are employed. Computational studies on mechanisms, reactivities, and site selectivities in C−H functionalization with other templates are currently underway in our laboratories.

■ ASSOCIATED CONTENT

⑤ Supporting Information

Complete ref 15; additional text, six figures, one scheme, and six tables with details on distortion/interaction analysis and MP2 and CCSD(T) benchmark results; and Cartesian coordinates of optimized structures. This material is available free of charge via the Internet at http://pubs.acs.org.

■ AUTHOR INFORMATION

Corresponding Authors
chydwu@ust.hk
yu200@scripps.edu
houk@chem.ucla.edu

Author Contributions
[⊥]Y.-F.Y. and G.-J.C. contributed equally.

Notes
The authors declare no competing financial interest.

■ ACKNOWLEDGMENTS

■ REFERENCES

(1) (a) Shilov, A. E.; Shul'pin, G. B. *Chem. Rev.* **1997**, *97*, 2879. (b) Daugulis, O.; Do, H.-Q.; Shabashov, D. *Acc. Chem. Res.* **2009**, *42*, 1074. (c) Lyons, T. W.; Sanford, M. S. *Chem. Rev.* **2010**, *110*, 1147. (d) Engle, K. M.; Mei, T.-S.; Wasa, M.; Yu, J.-Q. *Acc. Chem. Res.* **2011**, *45*, 788. (e) Neufeldt, S. R.; Sanford, M. S. *Acc. Chem. Res.* **2012**, *45*, 936.

(2) (a) Colby, D. A.; Bergman, R. G.; Ellman, J. A. *Chem. Rev.* **2009**, *110*, 624. (b) Thalji, R. K.; Ahrendt, K. A.; Bergman, R. G.; Ellman, J. A. *J. Org. Chem.* **2005**, *70*, 6775. (c) Harada, H.; Thalji, R. K.; Bergman, R. G.; Ellman, J. A. *J. Org. Chem.* **2008**, *73*, 6772. (d) Kalyani, D.; Sanford, M. S. *Org. Lett.* **2005**, *7*, 4149. (e) Wang, C.; Chen, H.; Wang, Z.; Chen, J.; Huang, Y. *Angew. Chem., Int. Ed.* **2012**, *51*, 7242. (f) Wang, C.; Sun, H.; Fang, Y.; Huang, Y. *Angew. Chem., Int. Ed.* **2013**, *52*, 5795.

(3) (a) Ciana, C.-L.; Phipps, R. J.; Brandt, J. R.; Meyer, F.-M.; Gaunt, M. J. *Angew. Chem., Int. Ed.* **2011**, *50*, 458. (b) Wang, X.; Leow, D.; Yu, J.-Q. *J. Am. Chem. Soc.* **2011**, *133*, 13864. (c) Guo, X.; Li, C.-J. *Org. Lett.* **2011**, *13*, 4977. (d) Wu, Z.; Luo, F.; Chen, S.; Li, Z.; Xiang, H.; Zhou, X. *Chem. Commun.* **2013**, *49*, 7653.

(4) (a) Phipps, R. J.; Gaunt, M. J. *Science* **2009**, *323*, 1593. (b) Duong, H. A.; Gilligan, R. E.; Cooke, M. L.; Phipps, R. J.; Gaunt, M. J. *Angew. Chem., Int. Ed.* **2011**, *50*, 463. (c) Chen, B.; Hou, X.-L.; Li, Y.-X.; Wu, Y.-D. *J. Am. Chem. Soc.* **2011**, *133*, 7668. (d) Zhang, Y.-H.; Shi, B.-F.; Yu, J.-Q. *J. Am. Chem. Soc.* **2009**, *131*, 5072. (e) Zhang, S.; Shi, L.; Ding, Y. *J. Am. Chem. Soc.* **2011**, *133*, 20218. (f) Leow, D.; Li, G.; Mei, T.-S.; Yu, J.-Q. *Nature* **2012**, *486*, 518. (g) Chotana, G. A.; Rak, M. A.; Smith, M. R. *J. Am. Chem. Soc.* **2005**, *127*, 10539. (h) Murphy, J. M.; Liao, X.; Hartwig, J. F. *J. Am. Chem. Soc.* **2007**, *129*, 15434. (i) Cho, J.-Y.; Tse, M. K.; Holmes, D.; Maleczka, R. E.; Smith, M. R. *Science* **2002**, *295*, 305. (j) Saidi, O.; Marafie, J.; Ledger, A. E. W.; Liu, P. M.; Mahon, M. F.; Kociok-Köhn, G.; Whittlesey, M. K.; Frost, C. G. *J. Am. Chem. Soc.* **2011**, *133*, 19298. (k) Hofmann, N.; Ackermann, L. *J. Am. Chem. Soc.* **2013**, *135*, 5877. (l) Lee, S.; Lee, H.; Tan, K. L. *J. Am. Chem. Soc.* **2013**, *135*, 18778.

(5) (a) Prüsse, T.; Lebrilla, C. B.; Drewello, T.; Schwarz, H. *J. Am. Chem. Soc.* **1988**, *110*, 5986. (b) Czekay, G.; Eller, K.; Schröder, D.; Schwarz, H. *Angew. Chem., Int. Ed.* **1989**, *28*, 1277. (c) Czekay, G.; Drewello, T.; Schwarz, H. *J. Am. Chem. Soc.* **1989**, *111*, 4561. (d) Schwarz, H. *Acc. Chem. Res.* **1989**, *22*, 282.

(6) (a) Stephenson, T. A.; Morehouse, S. M.; Powell, A. R.; Heffer, J. P.; Wilkinson, G. *J. Chem. Soc.* **1965**, 3632. (b) Skapski, A. C.; Smart, M. L. *J. Chem. Soc. D* **1970**, 658b. (c) Bakhmutov, V. I.; Berry, J. F.; Cotton, F. A.; Ibragimov, S.; Murillo, C. A. *Dalton Trans.* **2005**, 1989.

(7) (a) Davies, D. L.; Donald, S. M. A.; Macgregor, S. A. *J. Am. Chem. Soc.* **2005**, *127*, 13754−13755. (b) Garcia-Cuadrado, D.; Braga, A. A. C.; Maseras, F.; Echavarren, A. M. *J. Am. Chem. Soc.* **2006**, *128*, 1066−1067. (c) Lafrance, M.; Rowley, C. N.; Woo, T. K.; Fagnou, K. *J. Am. Chem. Soc.* **2006**, *128*, 8754−8756. (d) Garcia-Cuadrado, D.; de Mendoza, P.; Braga, A. A. C.; Maseras, F.; Echavarren, A. M. *J. Am. Chem. Soc.* **2007**, *129*, 6880−6886. (e) Lafrance, M.; Gorelsky, S. I.; Fagnou, K. *J. Am. Chem. Soc.* **2007**, *129*, 14570−14571. (f) Gorelsky, S. I.; Lapointe, D.; Fagnou, K. *J. Am. Chem. Soc.* **2008**, *130*, 10848−10849. (g) Rousseaux, S.; Gorelsky, S. I.; Chung, B. K. W.; Fagnou, K. *J. Am. Chem. Soc.* **2010**, *132*, 10692−10705. (h) Balcells, D.; Clot, E.; Eisenstein, O. *Chem. Rev.* **2010**, *110*, 749−823. (i) Ke, Z.; Cundari, T. R. *Organometallics* **2010**, *29*, 821−834. (j) Musaev, D. G.; Kaledin, A.; Shi, B.-F.; Yu, J. Q. *J. Am. Chem. Soc.* **2012**, *134*, 1690−1698. (k) Figg, T. M.; Wasa, M.; Yu, J.-Q.; Musaev, D. G. *J. Am. Chem. Soc.* **2013**, *135*, 14206−14214.

(8) (a) Ryabov, A. D.; Sakodinskaya, I. K.; Yatsimirsky, A. K. *J. Chem. Soc., Dalton Trans.* **1985**, 2629−2638. (b) Gomez, M.; Granell, J.; Martinez, M. *J. Chem. Soc., Dalton Trans.* **1998**, 37−43. (c) Dick, A. R.; Kampf, J. W.; Sanford, M. S. *J. Am. Chem. Soc.* **2005**, *127*, 12790−12791. (d) Giri, R.; Liang, J.; Lei, J. G.; Li, J. J.; Wang, D. H.; Chen, X.; Naggar, I. C.; Guo, C. Y.; Foxman, B. M.; Yu, J. Q. *Angew. Chem., Int. Ed.* **2005**, *44*, 7420−7424. (e) Giri, R.; Chen, X.; Yu, J. Q. *Angew. Chem., Int. Ed.* **2005**, *44*, 2112−2115. (f) Powers, D. C.; Ritter, T. *Nat. Chem.* **2009**, *1*, 302−309. (g) Powers, D. C.; Geibel, M. A. L.; Klein, J. E. M. N.; Ritter, T. *J. Am. Chem. Soc.* **2009**, *131*, 17050−17051. (h) Khusnutdinova, J. R.; Rath, N. P.; Mirica, L. M. *J. Am. Chem. Soc.* **2010**, *132*, 7303−7305.

(9) Giri, R.; Lan, Y.; Liu, P.; Houk, K. N.; Yu, J.-Q. *J. Am. Chem. Soc.* **2012**, *134*, 14118.

(10) For the crystallographic structure of trinuclear palladium acetate obtained from CH_2Cl_2, see (a) Cotton, F. A.; Han, S. *Rev. Chim. Miner.* **1985**, *22*, 277. (b) Stephens, T. A.; Morehous, S. M.; Powell, A. R.; Heffer, J. P.; Wilkinson, G. *J. Chem. Soc.* **1965**, 3632. (c) Skapski, A. C.; Smart, M. L. *J. Chem. Soc. D* **1970**, 658. (d) Bakhmutov, V. I.; Berry, J. F.; Cotton, F. A.; Ibragimov, S.; Murillo, C. A. *Dalton Trans.* **2005**, 1989.

(11) (a) Bercaw, J. E.; Durrell, A. C.; Gray, H. B.; Green, J. C.; Hazari, N.; Labinger, J. A.; Winkler, J. R. *Inorg. Chem.* **2010**, *49*, 1801. (b) Engle, K. M.; Mei, T.-S.; Wasa, M.; Yu, J.-Q. *Acc. Chem. Res.* **2011**, *45*, 788. (c) Callear, S.; Spencer, J.; Patel, H.; Deadman, J.; Hursthouse, M. *J. Chem. Crystallogr.* **2011**, *41*, 523. (d) Selbin, J.; Abboud, K.; Watkins, S. F.; Gutierrez, M. A.; Fronczek, F. R. *J. Organomet. Chem.* **1983**, *241*, 259.

(12) (a) Cotton, F. A.; Koshevoy, I. O.; Lahuerta, P.; Murillo, C. A.; Sanaú, M.; Ubeda, M. A.; Zhao, Q. *J. Am. Chem. Soc.* **2006**, *128*, 13674. (b) Deprez, N. R.; Sanford, M. S. *J. Am. Chem. Soc.* **2009**, *131*, 11234. (c) Powers, D. C.; Xiao, D. Y.; Geibel, M. A. L.; Ritter, T. *J. Am. Chem. Soc.* **2010**, *132*, 14530. (d) Powers, D. C.; Ritter, T. *Acc. Chem. Res.* **2011**, *45*, 840. (e) Callear, S.; Spencer, J.; Patel, H.; Deadman, J.; Hursthouse, M. *J. Chem. Crystallogr.* **2011**, *41*, 523.

(13) Tan, Y.; Barrios-Landeros, F.; Hartwig, J. F. *J. Am. Chem. Soc.* **2012**, *134*, 3683.

(14) Sanhueza, I. A.; Wagner, A. M.; Sanford, M. S.; Schoenebeck, F. *Chem. Sci.* **2013**, *4*, 2767.

(15) Frisch, M. J. et al. *Gaussian 09, Revision C.01*; Gaussian, Inc., Wallingford, CT, 2010.

(16) (a) Becke, A. D. *J. Chem. Phys.* **1993**, *98*, 5648. (b) Lee, C.; Yang, W.; Parr, R. G. *Phys. Rev. B* **1988**, *37*, 785. (c) Becke, A. D. *J. Chem. Phys.* **1993**, *98*, 1372. (d) Stephens, P. J.; Devlin, F. J.; Chabalowski, C. F.; Frisch, M. J. *J. Phys. Chem.* **1994**, *98*, 1623.

(17) (a) Hay, P. J.; Wadt, W. R. *J. Chem. Phys.* **1985**, *82*, 299. (b) Roy, L. E.; Hay, P. J.; Martin, R. L. *J. Chem. Theory Comput.* **2008**, *4*, 1029. (c) Ehlers, A. W.; Böhme, M.; Dapprich, S.; Gobbi, A.; Höllwarth, A.; Jonas, V.; Köhler, K. F.; Stegmann, R.; Veldkamp, A.; Frenking, G. *Chem. Phys. Lett.* **1993**, *208*, 111.

(18) (a) Ditchfield, R.; Hehre, W. J.; Pople, J. A. *J. Chem. Phys.* **1971**, *54*, 724. (b) Hehre, W. J.; Ditchfield, R.; Pople, J. A. *J. Chem. Phys.* **1971**, *54*, 2257. (c) Hariharan, P. C.; Pople, J. A. *Theor. Chim. Acta.* **1973**, *28*, 213.

(19) Zhao, Y.; Truhlar, D. G. *Theor. Chem. Acc.* **2008**, *120*, 215.

(20) (a) Dolg, M.; Wedig, U.; Stoll, H.; Preuss, H. *J. Chem. Phys.* **1987**, *86*, 866. (b) Andrae, D.; Häußermann, U.; Dolg, M.; Stoll, H.; Preuß, H. *Theor. Chem. Acc.* **1990**, *77*, 123.

(21) Krishnan, R.; Binkley, J. S.; Seeger, R.; Pople, J. A. *J. Chem. Phys.* **1980**, *72*, 650.

(22) Møller, C.; Plesset, M. S. *Phys. Rev.* **1934**, *46*, 618.

(23) Pople, J. A.; Head-Gordon, M.; Raghavachari, K. *J. Chem. Phys.* **1987**, *87*, 5968.

(24) Marenich, A. V.; Cramer, C. J.; Truhlar, D. G. *J. Phys. Chem. B* **2009**, *113*, 6378.

(25) Legault, C. Y. *CYLView, 1.0b*; Université de Sherbrooke, Canada, 2009; http://www.cylview.org.

(26) (a) Winstein, S.; Traylor, T. G. *J. Am. Chem. Soc.* **1955**, *77*, 3747. (b) Ackermann, L. *Chem. Rev.* **2011**, *111*, 1315. (c) Lapointe, D.; Fagnou, K. *Chem. Lett.* **2010**, *39*, 1118. (d) Gomez, M.; Granell, J.; Martinez, M. *Organometallics* **1997**, *16*, 2539. (e) Gómez, M.; Granell, J.; Martinez, M. *J. Chem. Soc., Dalton Trans.* **1998**, 37. (f) Biswas, B.; Sugimoto, M.; Sakaki, S. *Organometallics* **2000**, *19*, 3895. (g) Davies, D. L.; Donald, S. M. A.; Macgregor, S. A. *J. Am. Chem. Soc.* **2005**, *127*, 13754. (h) Tunge, J. A.; Foresee, L. N. *Organometallics* **2005**, *24*, 6440.

(27) Both geminal *i*-Bu- and methyl-substituted templates are highly *meta*-selective. The *i*-Bu gives slightly higher *meta*-selectivity (m:p:o = 95:4:1) than the methyl-subtituted template (m:p:o = 91:7:2). The less computationally demanding methyl-substituted template was used in computations.

(28) The transition state for the electrophilic substitution pathway II could not to be located. The Pd and C atoms always move away from each other during geometry optimizations of a potential intermediate. Therefore, we anticipate pathway II is unfavorable.

(29) (a) Stahl, S. S. *Angew. Chem., Int. Ed.* **2004**, *43*, 3400. (b) Gligorich, K. M.; Sigman, M. S. *Angew. Chem., Int. Ed.* **2006**, *45*, 6612. (c) Piera, J.; Backvall, J.-E. *Angew. Chem., Int. Ed.* **2008**, *47*, 3506.

(30) There are sixteen (2^4) conformations for *meta*-C−H activation; 16 conformations for *ortho*-C−H activation; eight conformations for *para*-C−H bond activation (since there is only one *para*-C−H); and three conformations in which the nitrile group does not coordinate to the Pd center. See Supporting Information for details.

(31) (a) Zhao, Y.; Truhlar, D. G. *Acc. Chem. Res.* **2008**, *41*, 157. (b) Zhao, Y.; Truhlar, D. G. *J. Chem. Theory Comput.* **2009**, *5*, 324. (c) Zhao, Y.; Truhlar, D. G. *Chem. Phys. Lett.* **2011**, *502*, 1. (d) Chen, P.; Dougan, B. A.; Zhang, X.; Wu, Y.-D.; Xue, Z.-L. *Polyhedron* **2013**, *58*, 30.

(32) (a) Wu, T.; Mu, X.; Liu, G. *Angew. Chem., Int. Ed.* **2011**, *50*, 12578. (b) Wan, J.-C.; Huang, J.-M.; Jhan, Y.-H.; Hsieh, J.-C. *Org. Lett.* **2013**, *15*, 2742.

(33) (a) Neo, Y. C.; Vittal, J. J.; Hor, T. S. A. *J. Chem. Soc., Dalton Trans.* **2002**, 337. (b) Kozitsyna, N. Y.; Nefedov, S. E.; Klyagina, A. P.; Markov, A. A.; Dobrokhotova, Z. V.; Velikodny, Y. A.; Kochubey, D. I.; Zyubina, T. S.; Gekhman, A. E.; Vargaftik, M. N.; Moiseev, I. I. *Inorg. Chim. Acta* **2011**, *370*, 382.

(34) (a) Ara, I.; Berenguer, J. R.; Eguizábal, E.; Forniés, J.; Lalinde, E.; Martín, A.; Martínez, F. *Organometallics* **1998**, *17*, 4578. (b) Braunstein, P.; Chetcuti, M. J.; Welter, R. *Chem. Commun.* **2001**, 2508. (c) Chouzier, S.; Gruber, M.; Djakovitch, L. *J. Mol. Catal. A: Chem.* **2004**, *212*, 43. (d) Kodanko, J. J.; Xu, D.; Song, D.; Lippard, S. J. *J. Am. Chem. Soc.* **2005**, *127*, 16004. (e) Tsai, C.-C.; Shih, W.-C.; Fang, C.-H.; Li, C.-Y.; Ong, T.-G.; Yap, G. P. A. *J. Am. Chem. Soc.* **2010**, *132*, 11887. (f) Pérez-Temprano, M. H.; Casares, J. A.; de Lera, Á. R.; Álvarez, R.; Espinet, P. *Angew. Chem., Int. Ed.* **2012**, *51*, 4917. (g) Cao, W.; Liu, X.; Peng, R.; He, P.; Lin, L.; Feng, X. *Chem. Commun.* **2013**, *49*, 3470. (h) Sun, S.; Sun, Q.; Zhao, B.; Zhang, Y.; Shen, Q.; Yao, Y. *Organometallics* **2013**, *32*, 1876. (i) York, J. T.; Llobet, A.; Cramer, C. J.; Tolman, W. B. *J. Am. Chem. Soc.* **2007**, *129*, 7990. (j) Koszinowski, K.; Schröder, D.; Schwarz, H. *J. Am. Chem. Soc.* **2003**, *125*, 3676. (k) González-Pérez, A. B.; Álvarez, R.; Faza, O. N.; de Lera, Á. R.; Aurrecoechea, J. M. *Organometallics* **2012**, *31*, 2053.

(35) Olson, L. P.; Whitcomb, D. R.; Rajeswaran, M.; Blanton, T. N.; Stwertka, B. *J. Chem. Mater.* **2006**, *18*, 1667.

(36) Ess, D. H.; Houk, K. N. *J. Am. Chem. Soc.* **2008**, *130*, 10187.